Astron. Astrophys. 298, 688–698 (1995)

ASTRONOMY AND ASTROPHYSICS

# Simultaneous optical and gamma–ray flaring in PKS 0420−014*

## Implications for emission processes and rotating jet models

**Stefan J. Wagner[1], Max Camenzind[1], Oliver Dreissigacker[1], Ulf Borgeest[2], Silke Britzen[3], Wolfgang Brinkmann[4], Ulrich Hopp[5], K.-Jochen Schramm[2,6], and Joachim von Linde[2]**

[1] Landessternwarte Königstuhl, D-69117 Heidelberg, Germany
[2] Sternwarte Hamburg, Gojenbergsweg 112, D-21029 Hamburg, Germany
[3] MPIfR, Auf dem Hügel 69, D-53121 Bonn, Germany
[4] MPE, Karl-Schwarzschild Str. 1, D-85740 Garching, Germany
[5] MPIA, Königstuhl 17, D-69117 Heidelberg, Germany
[6] Institut d'Astrophysique, 5 Ave Cointe, B-4000 Liège, Belgium

Received 8 June 1994 / Accepted 27 November 1994

**Abstract.** The flat-spectrum radio quasar PKS 0420-014 has been identified as a variable gamma–ray source in the 100 MeV to 5 GeV energy band. We studied the variations of this object in the optical frequency regime, and found pronounced flares. The highest gamma–ray flux densities were recorded during the most prominent flare in the optical range observed to date. Non-detections at gamma–ray energies coincide with low states on the optical flux.

A compilation of historical data is used to construct the overall spectrum, derive broad-band spectral indices from simultaneous measurements and describe them by a model which assumes a synchrotron cut-off in the optical range. The gamma–ray emission is created by inverse Compton scattering of the radiation from hot circumnuclear dust. These photons are scattered by those electrons which are producing the synchrotron radiation of the simultaneous optical flare.

Geodetic VLBI experiments are used to derive maps which clearly show superluminal motion of a knot on a curved trajectory. Both, the core component and the knot vary in flux.

The optical light curve is drastically undersampled but consistent with the assumption of repeated outbursts at 13 month intervals. This may be an indication that the flares are caused by a knot of enhanced particle density propagating on a helical trajectory in a rotating jet.

**Key words:** radiation mechanisms: non-thermal – active galaxies – galaxies: jets – quasars: individual PKS 0420-014 – gamma rays: observations – radio continuum: galaxies

### 1. Introduction

Flat-spectrum radio sources are known to be variable at GHz frequencies, where the emission originates predominantly from a compact, self-absorbed core and a compact jet. These active galactic nuclei form the parent population of those objects which have been identified as emitters of high-energy gamma rays in the 30 MeV - 10 GeV regime. The EGRET instrument on board the Compton Gamma Ray Observatory (CGRO) satellite has discovered 24 such objects during its 15 months all sky survey (Fichtel et al. 1994). Significant variability was found for some of these objects both within an individual 2-3 week CGRO observation and between repeated pointings (Michelson et al. 1994). In order to discriminate between various suggestions for the emission mechanisms of the high-energy photons, it is important to investigate whether the variability at these high energies is correlated with variations at lower frequencies. Such a correlation is predicted by the commonly favoured explanation suggesting that the gamma–ray photons were Compton-scattered off the relativistic electrons of the jet. Both, the comptonization of those photons which were emitted by the scattering electrons in the first place via the synchrotron process (SSC models, e.g. Maraschi et al. 1992) as well as of ambient photons (e.g. Dermer & Schlickeiser 1993; Sikora et al. 1994) have been discussed.

Lags, or – more generally – the transfer function between outbursts of low-energy radiation and gamma emission constrain the source geometry, the relative location of the sites of emission at the two frequencies, and acceleration and cooling time scales. Variations of the synchrotron emis-

*Send offprint requests to*: S. Wagner, e-mail: swagner@hp2.lsw.uni-heidelberg.de

* Partly based on observations collected at the German-Spanish Astronomical Centre, Calar Alto, operated by the Max-Planck-Institut für Astronomie (MPIA), Heidelberg, jointly with the Spanish National Commission for Astronomy and partly based on data collected at the European Southern Observatory, Chile.

sion have been studied at radio, sub-mm, and optical frequencies. Although several sources have been found which show a close correspondence between radio emission and optical variations (e.g. Balonek & Dent 1980; Quirrenbach et al. 1991; Wagner & Witzel 1992), the latter may be a better indicator of synchrotron variations in those sources where the dominant contribution at radio frequencies is self-absorbed.

Synchrotron emission from blazars at optical frequencies is emitted in the optically thin regime and acts as an ideal tracer. Therefore, we have used optical monitoring to test the prediction that jets, which are supposed to be the sites of the flaring component in flat-spectrum quasars, are rotating about their axis due to the conservation of angular momentum carried by the accreted plasma. In such a scenario, density perturbations within the jet travel on helical paths. If the fluid moves relativistically, the emission is beamed into the forward direction. This direction of enhanced emission changes and hence its inclination to the fixed line-of-sight towards an external observer varies (Camenzind & Krockenberger 1992). This will cause variations of observed flux density even if the radiation emitted from the knot of enhanced density is constant in the rest frame of the jet. It provides a natural mechanism for the suggestion that the symmetric light curves of variable flat-spectrum radio sources may largely be due to geometric modulations (Wagner 1991). Observations of 3C 345 are in accordance with such a scenario (Schramm et al. 1993), and we suggest that PKS 0420-014 shows similar signatures in its light curve.

PKS 0420-014 (z=0.915) has been studied extensively at many wavelengths and the historic data base is used to construct broadband electromagnetic spectra during the quiescent and flaring states. The source has always shown high degrees of polarization (up to 17 %) in the optical regime (Wills et al. 1992). Its very compact nature is evident from the rapid variations in all frequency bands, and is confirmed by the new VLBI observations presented here.

## 2. Observations and reductions

The Quasar PKS 0420-014 has been observed during the Hamburg Quasar Monitoring Program (HQM, Borgeest & Schramm 1994) which aimed at an identification of flares caused by gravitational microlensing. Since its detection as an emitter of high-energy radiation, it has also been observed repeatedly at the Landessternwarte in Heidelberg as part of a coordinated monitoring program of gamma–ray blazars (Wagner et al., in preparation). Additional observations have been performed during other campaigns. The HQM data were taken with the 1.23 m telescope on Calar Alto and the 0.9 m 'Dutch' telescope on La Silla (March 1992). They were analyzed as described by Borgeest & Schramm (1994). The Heidelberg data were taken with a CCD-equipped 0.7 m telescope at the Landessternwarte and were reduced together with the additional measurements, taken at the 2.2 m and 3.5 m telescope of Calar Alto observatory using the software developed for Intraday variability monitoring (e.g. Wagner 1991). All measurements were taken with R band filters, however, both Johnson and Cousins filter systems were used in the different programs. Since there are no strong emission lines in those wavelength regimes where Johnson and Cousins filters do not overlap, the differences introduced by the filter systems can be calibrated easily.

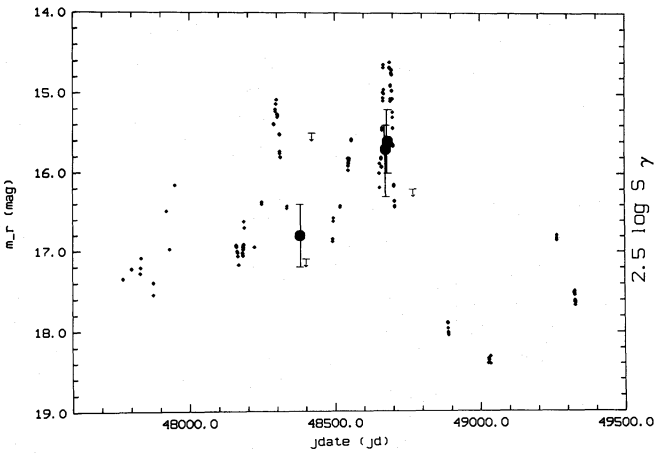


**Fig. 1.** Light curve of PKS 0420-014 at 650 nm (R band: small dots, errors are smaller than symbols) and in the range 100 MeV – 5 GeV (EGRET regime: full dots, arrows). Gamma–ray flux densities are displayed on a logarithmic scale to enable a better comparison

## 3. Optical variations

The optical light curve is displayed in Fig. 1. Three major outbursts lasting about one month each can be identified at the beginning of 1990, 1991 and 1992. In addition to these well-defined flares, variations at even shorter time scales seem to be superposed. The amplitude of this flickering is almost comparable to the well-defined flares, but the time scales are significantly shorter and the total energy emitted during one of the fast spikes is orders of magnitudes less than the energy emitted by a well-defined flare. The power density spectrum shows a strong signal at a frequency corresponding to 1 $yr^{-1}$. Since the window function is not influenced significantly by the annual interruption of sun-blockage, there is a clear indication for a preferred time scale in this limited data-set. Most of the power of the variations, however, resides on short time-scales ($1d < dt < 10d$). In spite of the limited statistics, our measurement accuracy of 0.01 mag allows us to trace variability to time scales as short as 3 hours. On time scales shorter than 1000 sec, variations are comparable to our measurement errors.

## 4. Gamma–ray flares

Radecke et al. (1994) reported results from two observations of PKS 0420-014 with the EGRET instrument during the CGRO full-sky survey. Information about an earlier pointing was taken from Fichtel et al. 1994. During the observation in Feb./March 1992 (JD 2 448 672 – 2 448 685) the source was detected at a flux level of $5 \pm 1.4 \cdot 10^{-7}\ \gamma\ cm^{-2}\ s^{-1}$ ($E > 100$ MeV). Radecke et al. (1994) mention indications for variability from the 20 % rise

($4.6\pm1.8 \cdot 10^{-7}$ to $5.4\pm1.9 \cdot 10^{-7}$ $\gamma$ cm$^{-2}$ s$^{-1}$) during the two weeks of the entire pointing. In May/June 1992 (JD 2 448 780 – 2 448 800) the source was observed, but not detected with an upper limit (95% confidence) of S (E > 100 MeV) < $3.6 \cdot 10^{-7}$ $\gamma$ cm$^{-2}$ s$^{-1}$. The epochs of these observations are indicated in Fig. 1. The scaling of the $\gamma$ flux densities is logarithmic. It is obvious that the epoch of gamma–ray detection from PKS 0420-014 coincides with the strongest outburst of optical emission observed in our 5 years of monitoring since 1989. To our knowledge, PKS 0420-014 has never been observed in a brighter state in the optical regime (for a long-term study see the light curve of Smith et al. 1990). This strengthens the identification of PKS 0420-014 as the gamma-ray source at this position. An expanded portion of Fig. 1, the months of February and March 1992, is shown in Fig. 2.

Unfortunately, no optical observations were performed exactly during the gamma–ray detection. It is, therefore, not possible to correlate the weak indication of gamma–ray flux-density variability during this epoch with changes in the optically thin synchrotron branch. If the optical flare had a simple, symmetrically peaked shape, it is likely that the peak of the synchrotron flare occurred at a time when the gamma flare was still rising. During the May/June 1992 epoch PKS 0420-014 was only 32° away from the sun which did not enable us to perform any simultaneous optical measurements. A smooth extrapolation of the light curve would indicate, however, that the fluxes in the optical regime were probably lower by a factor of 4 compared to the state in Feb./March. If the amplitudes of variability in the optical frequency domain and at gamma–ray energies would scale linearly, the above extrapolation would be consistent with the upper limit of the gamma–ray observations.

Fichtel et al. (1994) report earlier observations with EGRET showing a positive detection at a flux level of S (E > 100 MeV) = $0.19 \pm 0.07 \cdot 10^{-6}$ $\gamma$ cm$^{-2}$ s$^{-1}$, and upper limits of S (E > 100 MeV) < $0.14, 0.6 \cdot 10^{-6}$ $\gamma$ cm$^{-2}$ s$^{-1}$ during the epochs April 22 - May 7, May 16 - May 30 and June 8 - June 15, 1991, respectively. Unfortunately, all of these measurements have been taken when the sun was too close to the object to perform optical measurements. The extrapolation of the optical flare in February 1991 indicates however, that the optical flux - level was declining during these three epochs (Fig. 1).

The second important aspect of the simultaneous observations is the ratio of the energy densities in the optical and gamma–ray ranges $\nu S_\nu$ ($10^{14.7}$ Hz) / $\nu S_\nu$ ($10^{23}$ Hz) which is 0.25, much larger than earlier claims which suggested that, in EGRET-detected AGN, the gamma–ray regime is more luminous by several orders of magnitude than any other band. In view of the large variations in amplitude of optical and gamma–ray flux densities, truly simultaneous observations are required to derive $S_{opt}$ / $S_\gamma$.

## 5. Broadband spectrum

The entire electromagnetic spectrum has to be covered to understand the radiation mechanisms in objects whose energy is emitted over such a wide range in frequency. Unfortunately, it has not been possible to measure a simultaneous spectrum of PKS 0420-014 at any given epoch. Radecke et al. (1994) compiled data from the literature to construct a broadband spectrum which is not simultaneous in time. We extend this compilation by including all data known to us. Being a bright quasar with a long record of variability studies, PKS 0420-014 has been included in many of the major monitoring programs and has been observed repeatedly with IRAS, X–ray satellites and EGRET. In Fig. 3 we display an overall spectrum which contains the highest and lowest fluxes at any given frequency reported in the literature. The references for all the relevant measurements of flux densities are listed in Table 1. In addition we used the flux densities reported in Kühr et al. (1981). The source spends 80 % of the time within one magnitude around the median brightness level and only 20 % in brighter stages. This illustrates that the variations are characterized by flares on top of a constant component rather than by oscillations around some level. Therefore the lower envelope of the overall spectrum is better defined than the upper one. Furthermore it is plausible that the full range is better explored in those frequency bands which have been investigated in long-term monitoring programs.

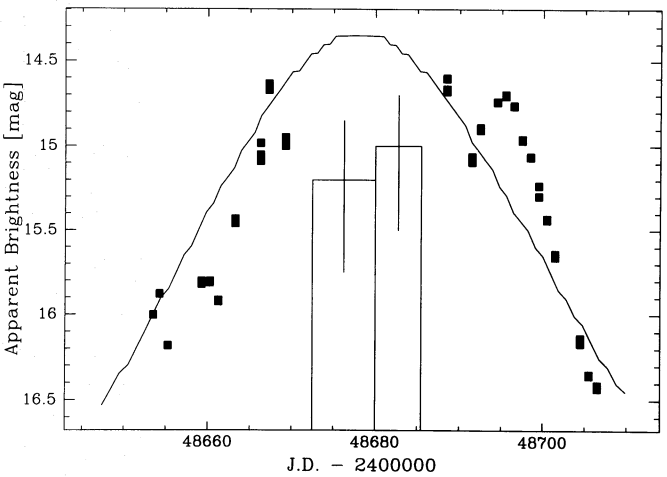


**Fig. 2.** The highest peak of the light curve shown in Fig. 1 compared to the gamma–ray fluxes (boxes, scaled arbitrarily). The thin line is a reproduction of the model discussed in Sect. 7 (see Fig. 5). The excess emission during decline is supposed to be due to additional flickering

### *5.1. Flux density measurements*

The flux density measurements were collected in various monitoring programs. PKS 0420-014 has been monitored in the Michigan programme at 4.8 - 14.5 GHz (Aller 1985). Variations in this frequency band are typical for HPQs (about a factor of 2 on time scales of a few years). The degree of polarization is variable between 1 and 3 %. The extreme flux density measurements were reported by Brown et al. (1989). The observations by the Metsähovi Radio Research Station (Teräsranta et al. 1992) at 22 and 37 GHz reveal variations between 3 and 7 Jy on time scales of about 500 days. Tornikoski et al. (1993) report on a wide range of flux density measurements from 2 to 230 GHz. Their

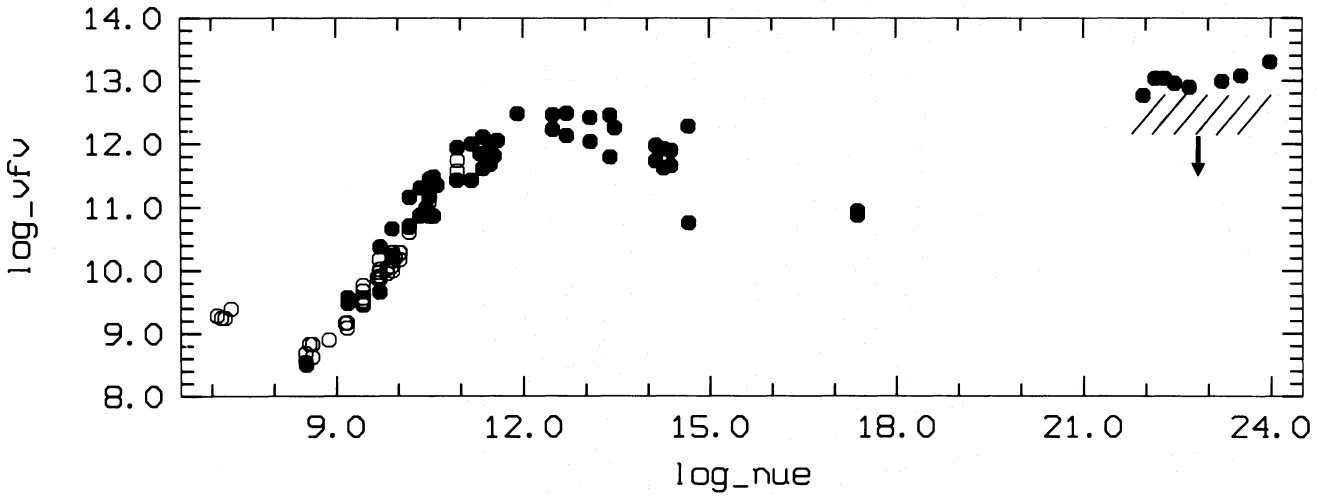


**Fig. 3.** Broadband spectrum of PKS 0420-014. In all energy bands the range of flux-densities reported in the literature is compiled. References to the full dots are given in Table 1, the rest is taken from Kühr et al. (1981). The hatched area in the high-energy domain represents the range of variability measured by EGRET. The lower bound is an upper limit

spectra reveal clearly that the amplitude of variation remains constant over two orders of magnitude in frequency into the sub-mm regime. The range of flux densities at higher frequencies is consistent with the range covered in the high-frequency monitoring of Steppe et al. (1993) and a few extreme flux values collected by Reich et al. (1993). Additional sub-mm observations at even higher frequencies were observed only at a few epochs which seem to remain in the range within the extrapolations from lower frequencies (see Fig. 3) except for the 370 $\mu$m observation by Gear et al. 1985. The maximum of the energy spectrum is indeed expected in this wavelength range, the measurement itself is fairly uncertain (3.7 $\pm$ 1.1 Jy). The 370 $\mu$m observation was taken simultaneously with the high state near-IR measurements.

During the IRAS mission several observations have been carried out in the survey and in pointed mode. The extreme values reported in the literature are listed in Table 1. The upper range traces a nearly flat energy spectrum throughout the mid-infrared. While Impey & Neugebauer 1988 have confirmed the significant variations in the IRAS flux-density measurements, they do not confirm the extremely high flux densities reported by Neugebauer et al. (1984). These high IRAS fluxes were taken during a period with clear optical activity. The sampling rate of the optical data has been to poor, however, to determine whether a strong flare occurred. We speculate that the high values indicate the maximum mid-IR level during extreme outbursts. Unfortunately no mid-IR measurements were taken during the extreme outburst reported in Sect. 1.

Only very few near-IR measurements have been reported in the literature. The range represented in Fig. 3 only represents two or three measurements in each of the three bands. It is very likely, therefore, that the actual variations span a much wider range in flux density, which may be comparable to that observed in the optical regime. However, this cannot be proven with the present data. Except for the measurements by Brindle et al. 1986, which are discussed below, we are not aware of strictly simultaneous optical observations at the epochs of the near-IR measurements.

The range in optical variations is fully covered by the variations observed in 1992 (see Fig. 1). In order to compare this range to the much longer sequence of observations taken by the Rosemary Hill Observatory (see e.g. Smith et al. 1990) we compared their photographic magnitudes with our R band CCD observations in early 1989. Since no colour measurements have been taken and due to the slightly different epochs the transformation is estimated to be no better than 0.3 mag. This does not affect the conclusion, that the total span in photographic magnitudes of the Rosemary Hill Observatory (P = $19\overset{m}{.}0$ to $16\overset{m}{.}2$) is comparable to the span observed in 1992 (R = $18\overset{m}{.}3$ to $14\overset{m}{.}6$).

References: 1) Gosh & Gopal-Krishna 1990. 2) Brown et al. 1989. 3) Impey & Tapia 1990. 4) Aller et al. 1985. 5) Reich et al. 1993. 7) M. Tornikoski, priv. comm. 8) Tornikoski et al. 1993. 9) Gear et al. 1986. 10) Steppe et al. 1993. 11) Gear et al. 1984. 12) Chini et al. 1989. 13) Gear et al. 1985. 14) Neugebauer et al. 1986. 15) Neugebauer et al. 1984. 16) Brindle et al. 1986. 17) this paper. 18) Worrall & Wilkes 1990. 19) Radecke et al. 1994.

Two epochs of X–ray observations have been reported. One of two *Einstein* observations has been too short to accumulate a sufficient amount of counts. The second *Einstein* observation is discussed e.g. by Worrall & Wilkes 1990, reporting a flat energy spectrum ($\alpha_E$=-0.15) and a flux density of 0.36 $\mu$Jy. During the 1990 ROSAT measurement reported by Brinkmann et al. (1994), the hardness ratios are consistent with a power law spectrum ($\alpha_E$=1) for a galactic value of $n_H$. The small number of photons does not allow accurate constraints on the spectral slope.

The range of variability in the gamma–ray range reported by Radecke et al. (1994), is illustrated by the hatched area in Fig. 3. No COMPTEL observations have been reported to date.

**Table 1.** References to upper and lower bounds from flux-density monitoring campaigns

| Reference | log $\nu$ (Hz) | log $\nu S_\nu$ |
|---|---|---|
| 1 | 8.51 | 8.50 |
| 2 | 9.18 | 09.48 - 09.57 |
| 2, 3 | 9.70 | 09.66 - 10.38 |
| 4 | 9.90 | 10.24 - 10.66 |
| 2, 4 | 10.18 | 10.71 - 11.16 |
| 2 | 10.36 | 10.88 - 11.31 |
| 5 | 10.51 | 11.18 - 11.45 |
| 7 | 10.57 | 10.86 - 11.48 |
| 8 | 10.95 | 11.43 - 11.94 |
| 9, 10 | 11.18 | 11.43 - 12.00 |
| 8 | 11.36 | 11.62 - 12.11 |
| 2, 11 | 11.48 | 11.68 - 12.02 |
| 12 | 11.54 | 11.81 |
| 13 | 11.59 | 12.05 |
| 13 | 11.91 | 12.48 |
| 14, 15 | 12.48 | 12.23 - 12.46 |
| 14, 15 | 12.70 | 12.13 - 12.48 |
| 14, 15 | 13.08 | 12.04 - 12.42 |
| 14, 15 | 13.40 | 11.80 - 12.45 |
| 13 | 13.48 | 12.26 |
| 13 | 14.13 | 11.74 - 11.98 |
| 13, 16 | 14.26 | 11.62 - 11.93 |
| 13 | 14.38 | 11.66 - 11.90 |
| 17 | 14.66 | 10.75 - 12.28 |
| 17, 18 | 17.38 | 10.88 - 10.95 |
| 19 | 21.96 - 23.99 | 12.77 - 13.30 |

### 5.2. *Spectral indices*

From the well-sampled light curves in the radio regime broadband spectral indices for many epochs can be derived. The envelope of the overall spectrum at $\lambda > 0.8$ mm indicates, however, that most of the flux is emitted from optically thick regions, such that variations are detected only with a certain time lag at these lower frequencies[1]. We therefore used the optical light curves to compute simultaneous spectral indices. The photographic measurements of Smith et al. (1990) cover more than 20 years and were connected to the R-band light curve shown in Fig. 1 as described in the previous section. This combined light curve shows no correlation with the light curves between 4.8 and 230 GHz (Aller et al. 1985; Teräsranta et al. 1992; Steppe et al. 1993).

During the IRAS observations 1983 and 1984, the light curve is not sampled in sufficient detail to obtain simultaneous mid-IR – optical spectral indices. Power law extrapolations of the most extreme IRAS spectral indices into the optical regime suggest fluxes at 650 nm, which are within the range of variations in the optical R band. There is no evidence against the assumption that the spectra between 100 $\mu$m and 650 nm are well-described by a power law. The spectral indices range between $\alpha_E = 1.02 \pm 0.07$ and $1.43 \pm 0.09$. During the only epoch known to us with simultaneous optical-IR measurements (Brindle et al. 1986) a break is indicated around 1 $\mu$m with $\alpha_E(1.64\,\mu\text{m} - 0.72\,\mu\text{m}) = 1.42 \pm 0.12$ (which could be extrapolated into the range of IRAS flux density measurements) and $\alpha_E(0.72\,\mu\text{m} - 0.55\,\mu\text{m}) = 0.83 \pm 0.13$.

The ROSAT observations were obtained at JD 2 448 115 - 2 448 119. Interpolating our R band observations taken less then a week before and after this date (Fig. 1) we derive an optical - X–ray slope of $\alpha_E = 1.0$, which is consistent with the X–ray spectral index and the optical slope measured by Brindle et al. (1986). Furthermore, the interpolated optical flux density is within the spectral extrapolation of the ROSAT observations. There are no indications of a UV/soft X–ray bump. We also estimated the optical flux at the epoch of the *Einstein* observation. The wider temporal spacing of the optical data only allow a rough estimate, resulting in a large uncertainty of the optical - X–ray spectral index ($\alpha_E = 1.0 \pm 0.3$). This is also consistent with the optical - X–ray slope during the ROSAT observations and shows again no evidence of a soft X–ray bump. If the mid-IR fluxes during the X–ray observations were within the range indicated in Fig. 3, the spectral indices in the optical - X–ray regime are inconsistent with the assumption of a smooth power law extending from 100 $\mu$m up to a few keV. They confirm the existence of a spectral break somewhere around 1 $\mu$m.

During its detection by EGRET, PKS 0420-014 underwent the strongest outburst at optical frequencies known to us. Unfortunately the rise and decay of this flare are covered much better than the maximum, which occurred during the EGRET observations. The energy ratio $(\nu S_\nu)_{\text{opt.}}/(\nu S_\nu)_\gamma \gtrsim 0.25$ derived from these measurements may be only a lower limit, if the peak of the optical flare exceeded the plateau sketched in Fig. 2. The upper limit to the gamma–ray flux in May/June 1992 would be consistent with the lower optical flux if the spectral index $\alpha_{\text{opt.}/\gamma}$ remained constant.

### 5.3. *Spectral components*

The radio spectrum has a lower envelope which is not well described by a power law. This indicates a superposition of several components (jet and core) which become opaque at different frequencies. The amplitudes of variations are as large as one order of magnitude. The high frequency peak illustrates that the core is optically thick at $\lambda > 300$ $\mu$m. Therefore, no direct correlations are expected between the optically thin high frequency tail of the synchrotron branch and the radio regime. In this particular object, one would not expect to find correlations of optical light curves even with mm- or sub-mm monitoring data (i.e. up to 230 GHz).

Due to the different sampling patterns, it is unclear whether the range in amplitudes actually decreases towards mm and sub-mm frequencies. The uncertainty of the 370 $\mu$m flux density observation does not allow any conclusion about a two component

[1] Dent et al. 1979 actually suggested a lag between the optical outbursts and those at 15 GHz of about 2 years, which is consistent with the lag between the optical flare in 1978 (Smith et al. 1990) and the high state at 8 GHz in 1979 - 1980 (Aller et al. 1985). In view of the rate of major flares, which is about $(2.5 \text{ years})^{-1}$, the coverage in frequency and time is too poor to derive the lag in a convincing way.

structure and a break in the sub-mm regime. The variability and spectral shapes of the IRAS observations exclude large contributions from thermal components.

The near-IR does not show a strong thermal component either. Brindle et al. 1986, report the polarization to be higher in the H band (13 %) than in the R band (11 %) in simultaneous measurements. Likewise, the lowest flux densities in the optical regime exclude *dominant* contributions from the host galaxy or thermal emission. PKS 0420-014 has been a HPQ in all polarization studies (Wills et al. 1992), confirming the dominant contribution from non-thermal processes.

The absence of a soft X–ray excess argues against strong contributions from hot plasma, but the spectral break in the optical regime also rules out any synchrotron model of a homogeneous component with a power law spectrum extending into the X–ray regime. This argues in favour of the assumption that the UV/X–ray part of the spectrum is due to inverse Compton-scattered radiation. The apparent energy-density of the gamma emission exceeds that of the IR - optical contribution, but the factor is less than 10. A correlation between the particles radiating at optical wavelengths and gamma–ray energies is implied from the correlated outbursts.

## 6. VLBI observations

Due to its suspected high degree of compactness the Quasar PKS 0420-014 was chosen for observation during the regular geodetic VLBI campaigns IRIS-S (*International Radio Interferometric Surveying*) and EUROPE. Both campaigns are performed regularly (IRIS-S monthly since 1980 and EUROPE four times per year since 1990) at the wavelength of 13 and 3.6 cm. Data spaced by about half a year taken between 1990.38 and 1992.15 observed at 3.6 cm by using the stations *Mojave*, USA, *Richmond*, USA, *Westford*, USA, *Wettzell*, Germany and *Harthebesthoeck*, South-Africa (yielding an angular resolution of 0.5 mas) were analyzed.

Details on the observations, calibrations and mapping are given in e.g. Schalinski (1985). Figure 4 shows the resulting maps for four observing epochs. PKS 0420-014 clearly shows a core-jet structure and exhibits structural variations. The distance between the northern *core*-component and the most intense secondary component increases with an annual rate of $\geq$0.15 mas/yr corresponding to 7.8 c at a distance of z = 0.915, $H_0$ = 50 km s$^{-1}$ Mpc$^{-1}$ and $q_o$ = 0.5. As illustrated in the maps and listed in Table 2, the secondary component changes its position angle, i.e. it does not move on a straight path. Furthermore, this bright knot varies in flux density by a factor of two between 1991.31 and 1992.15.

If the rate of expansion of the bright knot was 0.15 mas/yr on average, it was emitted in 1986. This coincides with a major outburst at GHz frequencies, as reported by Wehrle et al. (1992). Therefore, our result is in perfect agreement with the 5 GHz VLBI map shown by Wehrle et al. (1992). This map of the source at the epoch 1986.4 is unresolved for their beam of about 0.9 mas.

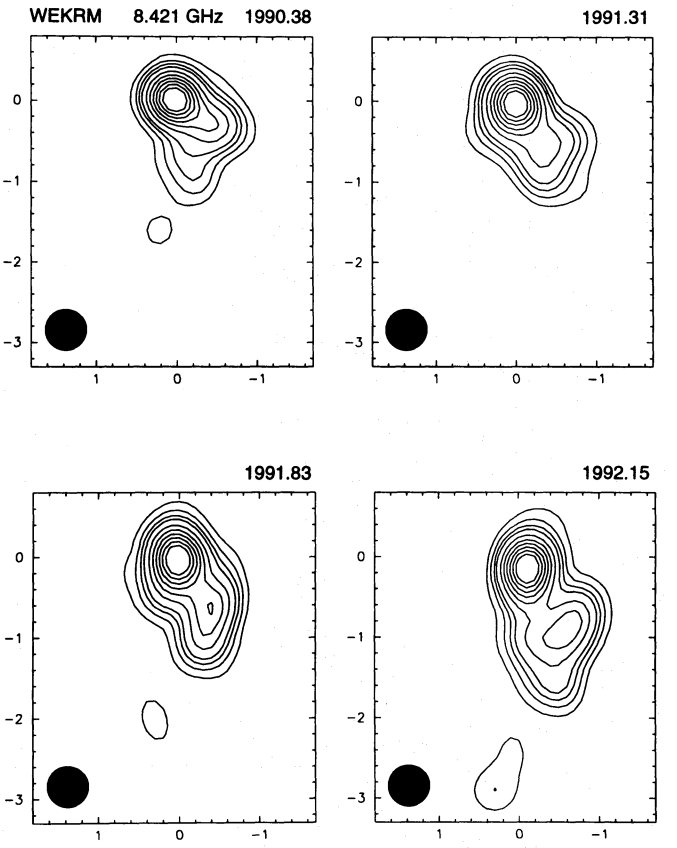


**Fig. 4.** VLBI maps at 8.42 GHz taken on 01/06/90, 07/05/91, 30/10/91, and 25/02/92, respectively. Relative distances are given in mas. Contours are 5, 10, 15, 20, 30, ..., 80 % of the peak brightness given for each map. Model fits are presented in Table 2

**Table 2.** Parameters of the three major components derived from model fits to the maps presented in Fig. 4 (Radius and P.A. refer to the relative orientation w.r.t. the core; FWHM, Rat., and p.a. refer to the average width, axis ratio and orientation of the individual components. $\triangle Flux$ = ±20%, $\triangle Radius$ = ±0.1$mas$, $\triangle P.A.$ = ±(5 − 10)°, $\triangle FWHM$ = ±10%, $\triangle Rat.$ = ±15% and $\triangle p.a.$ = ±20°.)

| Epoch | Flux [$Jy$] | Radius [$mas$] | P.A. [°] | FWHM [$mas$] | Rat. | p.a. [°] |
|---|---|---|---|---|---|---|
| 1990.38 | 1.6 | 0 | 0 | 0.2 | 0.7 | 25 |
| | 0.8 | 0.60 | 240 | 0.2 | 1 | 163 |
| | 0.3 | 1.7 | 178 | 0.2 | 1 | 72 |
| 1991.31 | 1.7 | 0 | 0 | 0.4 | 0.7 | 28 |
| | 0.5 | 0.72 | 221 | 0.5 | 1 | 166 |
| | 0.2 | 1.2 | 201 | 0.4 | 0.9 | 74 |
| 1991.83 | 1.5 | 0 | 0 | 0.4 | 0.7 | 8 |
| | 0.6 | 0.74 | 218 | 0.3 | 1 | 145 |
| | 0.3 | 1.2 | 199 | 0.1 | 1 | 143 |
| 1992.15 | 2.2 | 0 | 0 | 0.5 | 0.7 | 6 |
| | 0.9 | 0.87 | 218 | 0.3 | 1 | 142 |
| | 0.3 | 1.2 | 195 | 0.1 | 1 | 51 |

## 7. Are the flares due to knots moving in a rotating jet?

In spite of the poor sampling of the optical data, a regular spacing of the flares is indicated in Fig. 1. Regularly spaced outbursts and symmetric light curves have been found in rapidly variable BL Lac objects and 3C 345 (Wagner et al. 1993; Schramm et al. 1993). Such quasi–periodic flaring can be the result of a lighthouse effect due to the helical motion of the emitting knot moving within a given relativistic jet (Camenzind & Krockenberger 1992).

In the following we apply this lighthouse model of relativistic magnetized jets to explain the specific features in the light curve of Fig. 1. We assume the emitting knot to be a non–axisymmetric structure in the jet that is dragged along by the bulk motion $\beta_j$ of the jet material. Throughout the text indices k and j refer to the speed of the knot and the jet, respectively with $\beta = v/c$. The plasma flowing in the jet has still sufficient angular momentum to produce a rotational period which appears shortened by a factor $(1 - \beta_k \cos\Theta_j)(\simeq 1/300$ for $\Gamma_k = 16$ and $\Theta_j = 3^o)$ due to projection effects. The superposition of the outflow and rotational motion of the jet plasma results in a helical trajectory. The velocity vector of the knot sweeps around the jet axis producing a time–dependent Doppler boosting for an observer along a fixed line-of-sight. If the knot moves in a conical jet with opening angles less than 0.1 degree, the rotation around the central axis would produce a quasi–periodic flaring which ends abruptly when the opening slightly increases. In this model, the flares in the light curve are entirely due to variations of the effective Doppler boosting. For a given bulk motion of the knot ($\Gamma_k = 16$) and inclination of the jet ($\Theta_j = 2.9^o$), the observed rotation period determines the orbital radius R of the knot. Since major outbursts occur at intervals of about 13 months (see Fig. 1), we take this as the observed fundamental period for the rotation of the knot. We derive $R = 0.2$ light years and hence the mass of the central black hole, $M_H = 1.05 \cdot 10^{10}\, M_\odot$ (for $H_0 = 50$ km s$^{-1}$ Mpc$^{-1}$, $\Omega = 1$, $z = 0.915$).

The number of peaks in Fig. 1 is, however, not sufficiently restricted by the observations. There are three pronounced flares with steep increase and decrease in the flux and some shoulders preceding the peaks. The ambiguity introduced by the limited sampling implies that the parameters of the model cannot be fixed precisely. Since we do not aim at a perfect fit of the light curve but illustrate the similarity of the observed variations and those predicted by the scenario described above, we present three versions of different degrees of complexity. For the scales given above we matched the steep slopes by assuming a quite rapid rotation of the knot. This would imply that various peaks between the pronounced ones have been missed by the observations (dashed light curve in Fig. 5a). While this cannot be ruled out by the data, the solid line in Fig. 5a is based on the assumption that there are only three pronounced peaks. In this case, the flux boosting is amplified by the effect that the variation in the Doppler factor also boosts the synchrotron cutoff frequency back and forth through the optical window. By means of this effect, the amplitude of variation is increased by a factor of three in the optical regime. In this case, only the top of the peaks will

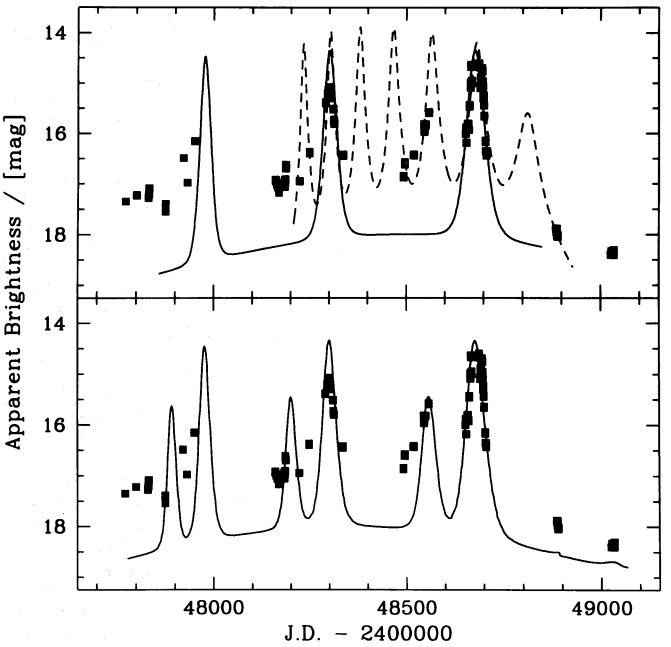


**Fig. 5. a** Model light curves for rotating knots which are assumed to move with $\Gamma_j = 16$ and $\Theta_j = 2.9^o$ in a jet with opening $0.06^o$. The dashed curve results for an orbital radius of the knot of 0.2 light years for a black hole mass of $M_H = 1.05 \cdot 10^{10}\, M_\odot$, the solid line is derived for a radius of 0.75 light years around a black hole with mass $M_H = 3.85 \cdot 10^{10}\, M_\odot$. **b** Model light curve resulting from the assumption of substructure within the emitting knot with two components travelling on the same path

be seen, the lower parts are blended by the steady jet emission. In this model the radius of the orbit of the knot is 0.75 light years (corresponding to an angular width of 0.04 mas) and the mass of the central black hole $M_H = 3.85 \cdot 10^{10}\, M_\odot$. The resulting light curve is very similar to the one derived for the 1991-1992 outburst in 3C 345 (Schramm et al. 1993; Camenzind 1994).

Several features in the light curve are not explained by this model. This is expected for the simple assumptions described above. It is unlikely that only a single, spherically symmetric density inhomogeneity exists within the jet. Elongated (banana–shaped) structures are expected if the knot is produced by some tearing instability in the jet. The superposition of emission from extended or many compact regions would give rise to additional humps in the light curve. This may explain the residuals to the fit in Fig. 5a. Naturally a more complex model with additional parameters provides a better fit to the actual light curves. This is illustrated in Fig. 5b. The data are compared with the prediction of a model, in which the single knot is composed of two distinct components travelling along the same path. Indications for an increase of the time interval between the main peak and its shoulder confirm the expected evolution of the spatial structure of the emitting knot, as it moves outwards along the jet.

The fits for the light curve can also explain the fairly symmetric structure of the peaks. In the context of the lighthouse model, the light curve of individual knots is almost symmetric in time. In Fig. 2 we show the theoretical light curve around

the third maximum compared to the observed data points. The overall fit is quite satisfactory except for an excess when the flux decreases. This could be due to an additional injection of particles in the knot.

The overall light curve has been derived under the assumption of a permanent injection of relativistic particles into the knot. Otherwise the flare would decay in the optical regime on a time scale of a few days due to synchrotron cooling. The decay time of the substructure $t_s \simeq (1+z)\,t'_s/\Gamma_k$ ($t'_s \simeq 4$ days) is of the order of a few days, which is in agreement with the parameters derived from the overall spectrum (i.e. a magnetic field strength $B' = 1.5$ Gauss and a maximum Lorentz factor of the electrons of $\gamma = (1-\beta^2)^{-1/2} = 3000$ - see Sect. 8).

The model is supported by the curved trajectory of the bright VLBI knot shown in Fig. 4. The observed superluminal motion implies $\Gamma_k > 8$, in agreement with our assumptions. If the repeated flares shown in Fig. 1, are due to a knot ejected in 1991, VLBI observations of 0.4 mas resolution should resolve this new feature in 1995.

## 8. Synchrotron emission and the source of gamma–rays in PKS 0420-014

In the following we discuss the possible origin of the global spectrum of this high–polarization quasar. Within the frame of the relativistic jet model discussed by Appl & Camenzind (1993: AC93a, b), the broadband spectrum of PKS 0420-014 follows from four basic assumptions:

- The outburst spectrum is due to knots moving relativistically in a strongly collimated jet on the parsec–scale. The relativistic electrons in the moving knots cool by emission of synchrotron photons and inverse Compton scattering.
- The total number density of the relativistic electrons in the knots, measured by the parameter $N_0 \simeq 5 \cdot 10^3$ cm$^{-3}$, is essentially given by the electron density in the jet.
- The underlying energy distribution of the electrons, $dN_e = N_0\,\gamma^{-p}\,d\gamma$, has a lower threshold of the Lorentz factors of the electrons of $\gamma_{\rm min} \simeq 10$, a primary injection spectral index $p \simeq 2.0$, a break due to cooling at $\gamma_b \simeq 100$ with spectral index $p_b = p+1$, and an upper cutoff $\gamma_c \leq 5000$ due to lack of further particle acceleration.
- The magnetic field which is needed for the synchrotron emission is helical and its strength is assumed to be given by a current $I_j \simeq 10^{17} - 10^{18}$ Ampères, corresponding to a typical magnetic field strength in the jet as measured in the quasar frame of reference (Camenzind 1993)

$$B_j \simeq \frac{2}{c}\frac{I_j}{R_j} \simeq 2\ \text{Gauss}\left(\frac{R_j}{0.1\ \text{light years}}\right)^{-1}\frac{I_j}{10^{18}\,A}\,. \quad (1)$$

The low–energy component of the spectrum is synchrotron emission originating in knots moving relativistically in the jet. The causal relation between radio outbursts and the appearance of VLBI knots has been demonstrated for various sources, such as 3C 273 (Krichbaum 1990), or 3C 345 (Babadzhanyants & Belokon 1986). As described in Sect. 6, the knot which is now observed with VLBI was ejected during the last major radio flare. The most natural source for the high–energy component visible at energies above a few MeV is upscattering of low–energy photons by the relativistic electrons in the knots of the jet. There are essentially two different sources for low–energy photons available in the central regions of active galaxies:

(1) Low–energy photons from the synchrotron emission itself (SSC models: e.g. Marscher & Gear 1985; Ghisellini & Maraschi 1989; Maraschi et al. 1992; Bloom & Marscher 1993; Marscher & Bloom 1993).
(2) External photon sources, such as direct radiation from the central accretion disk (Dermer et al. 1992; Dermer & Schlickeiser 1993), scattering of the UVX–bump radiation field by BLR emission clouds (Sikora et al. 1994), emission from stars and hot dust in the central part of the host galaxy (Camenzind & Dreissigacker, in preparation).

In the geometrical interpretation of the optical variability, which is described in Sect. 7, the synchrotron spectrum of PKS 0420-014 has a cutoff at $\nu_c \simeq 10^{14.5}$ Hz. Within this limit, SSC models cannot account for the high–energy emission up to energies of a few GeV (Fig. 3). Even a cutoff in the electron spectrum at $\gamma_c \simeq 10000$ would produce a corresponding cutoff in the inverse Compton spectrum at an energy of $E_c \simeq \gamma_c^2\,h\nu_c \simeq 100$ MeV. This is not sufficient to explain the spectrum observed by EGRET.

Higher energies can be achieved by inverse Compton processes on some source of external photons. Apart from the photon field from the nuclear source, the ambient radiation field provides source photons for inverse Compton scattering. Since the electrons in the jet flow outwards with relativistic speed (Doppler factor $D$), ambient radiation is blueshifted in the jet frame and produces Compton-scattered photons with even higher energies compared to those input photons emitted from the nucleus. The cutoff in the electron energy distribution will produce a corresponding cutoff $E_c$ in the observed gamma–ray spectrum at an energy

$$E_c \simeq \min\{D\,\gamma_c^2\,h\nu'_{\rm soft}\,,\ D\gamma_c m_e c^2\} < 45\,\text{GeV}\,\frac{D}{30}\,\frac{\gamma_c}{3000} \quad (2)$$

where $h\nu'_{\rm soft} = D\,h\nu_{\rm soft}$ is the typical energy of the soft energy spectrum as seen by the moving knot.

In order to dominate the synchrotron emission, the energy density $u'$ in the external photon field as measured in the frame comoving with the knot must exceed the energy density of the synchrotron radiation itself. Sikora et al. (1994) proposed that the external photons are due to UV photons from the central source which are scattered into the jet by BLR or intercloud plasma. This emission from the UVX–bump would produce an energy density $u'_{\rm sc}$ as observed in the frame of the moving knot

$$u'_{\rm sc} \simeq \Gamma_k^2\,\frac{\tau\,L_{\rm UVX}}{4\pi r^2 c} \simeq 10^{-3}\,\text{erg cm}^{-3}\,\Gamma_j^2\,\frac{\tau\,L_{\rm UVX}}{10^{12}\,L_\odot}\left(\frac{r}{\text{pc}}\right)^{-2} \quad (3)$$

decaying with $1/r^2$ as the knot moves away from the central source.

In Sect. 4 we suggested that the gamma outburst in March 1992 coincides with the optical peak. If this optical peak is actually emitted from the knot moving on a helical path as discussed in Sect. 7, the knot has already travelled a long distance away from the core, out to a radius where the energy density from scattered radiation has decayed. If gamma emission from comptonized ambient photons are related to outbursts lasting for more than one year, we need a photon field that is roughly spatially constant on a scale $d > 10$ parsecs. This follows from the fact that the observed travel time $t_k$ of the knot is drastically shortened by the relativistic projection effect

$$t_k = (1+z)(1-\beta_k \cos\Theta_j)\frac{d}{\beta_k c} \geq \frac{(1+z)}{2\Gamma_k^2}\frac{d}{\beta_k c} \qquad (4)$$

for small inclination angles $\Theta_j < 5$ deg. $\Gamma_k$ is the Lorentz factor for the knot motion and $\Theta_j$ the inclination angle between the line of sight and the velocity vector of the knot. For $\Gamma_k \simeq 10$ a considerable reduction results. The motion of a knot through the core of a large elliptical galaxy with core radius $R_c$ would correspond to a typical observed time–scale of a few years:

$$t_k \simeq \frac{(1+z)}{2}\,\mathrm{yr}\left(\frac{R_c}{30\,\mathrm{pc}}\right)\left(\frac{10}{\Gamma_k}\right)^2 . \qquad (5)$$

If the host galaxy of the quasar is a giant elliptical galaxy with $R_c \simeq 100$ pc (as discussed by Kormendy 1994), the natural photon source which remains constant over the inner jet region is the stellar light from the core and emission from hot dust located within the core. When the knot leaves this inner region, inverse Compton emission due to this soft photon field would rapidly drop.

As discussed by Camenzind & Dreissigacker (in preparation), the energy density in the diffuse stellar radiation field of the stellar core of the galaxy is not sufficient to provide a dense photon background field. Another source for an isotropic soft photon field is hot dust located within a region of $\simeq 30$ parsecs with energy density

$$u'_d \simeq \Gamma_k^2 \frac{L_d}{4\pi r_d^2 c}$$
$$\simeq 10^{-6}\,\mathrm{erg\,cm^{-3}}\,\Gamma_k^2 \frac{L_d}{10^{12}\,L_\odot}\left(\frac{r_d}{30\,\mathrm{pc}}\right)^{-2} . \qquad (6)$$

$L_d$ is the dust luminosity and $r_d$ the radius of the sphere where hot dust is located. Camenzind & Dreissigacker (in preparation) compare this energy density $u'_d$ in the photon field to the comoving energy density $u'_B$ in the magnetic field

$$u'_B = \frac{B'^2_j}{8\pi} \simeq \frac{u_B}{\Gamma_j^2} \simeq \frac{0.04}{\Gamma_j^2}\,\mathrm{erg\,cm^{-3}}\,B_j^2 \qquad (7)$$

for magnetic field strengths in the jet of the order of one Gauss and find

$$\frac{u'_d}{u'_B} \simeq 6\Gamma_k^4\left(\frac{R_j}{r_d}\right)^2 \frac{L_d}{10^{12}\,L_\odot}\left(\frac{I_j}{10^{18}\,A}\right)^{-2} , \qquad (8)$$

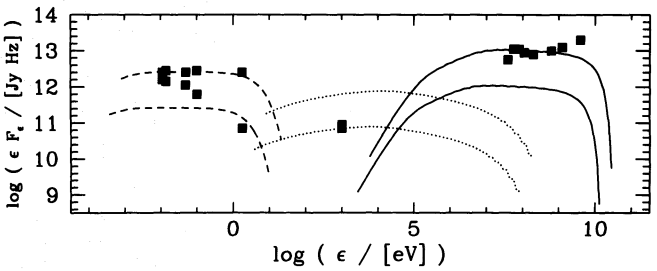


**Fig. 6.** Theoretical spectra for the quasar PKS 0420-014 compared to observed data points. The dashed lines show the self–absorbed synchrotron spectrum of the moving knot, the dotted lines the corresponding SSC branch and the thick lines inverse Compton emission from the same relativistic electron population in the knot produced by scattering on hot dust photons (with dust temperature $T_d = 2000$ K). The spectral fluxes for the high state are based on the following parameters: $\Gamma_j = 16$, $\Theta_j = 2.9^o$, $B'_j = 1.3$ Gauss, $p = 2.0$, $N_0 = 10^4$ cm$^{-3}$, $R_k = 0.025$ light years, $\gamma_b = 70$, $\gamma_c = 3000$

assuming that the jets on this scale are perfectly collimated into cylinders (AC93b). This ratio is in fact of order unity, or can even exceed one, whenever the dust sphere satisfies $r_d \leq \sqrt{6}\,\Gamma_k^2 R_j$. In this case, inverse Compton cooling dominates over synchrotron emission from the knot itself. Since the ratio between the energy densities varies with the fourth power of the bulk Lorentz factor $\Gamma_k$, this particular inverse Compton emission is only relevant for extremely relativistic jets, $\Gamma_k > 10$.

The global spectrum resulting from these considerations is shown in Fig. 6. The upper lines represent the spectrum at a time when the flux (dominated by the knot) reaches its maximum. The different branches are indicated by dashed, dotted and thick lines. The lower lines are a fit to a low state (as it occurred e.g. during the X–ray observations). The knot is assumed to move with a Lorentz factor $\Gamma_k = 16$ under a small inclination angle $\Theta_j = 2.9$ deg. Electrons are continuously accelerated in the knot with a power law of index $p = 2.0$. These electrons cool to a spectrum with energy index $p = 3.0$ beyond a Lorentz factor $\gamma_b = 70$. The observed flux in the synchrotron emission (dashed curve in Fig. 6) requires a total electron density $N_0 \simeq 10^{3.7}$ cm$^{-3}$. The sharp cutoff in the synchrotron spectrum in the optical region corresponds to a limit in the electron spectrum at $\gamma_c = 3000$. This cutoff in the synchrotron is required in order to understand the light curve in the optical domain. SSC emission (dotted curve) is always present, but cannot explain the EGRET data. The hard X–ray flux and the gamma–ray fluxes are explained in terms of the upscattering of hot dust photons (solid curve). In correspondence to the synchrotron spectrum, the inverse Compton spectrum would also have a sharp cutoff at about 5 GeV. For gamma rays occurring from dust photon scattering, the spectral index would be equal to the spectral index of the cooled synchrotron spectrum, $\alpha_\gamma \simeq -1.0$, while the spectral index in hard X–rays is flatter, $\alpha_X \simeq -0.5$. The spectrum in soft X–rays is due to SSC and is somewhat steeper than the spectrum in hard X–rays. This spectrum is able to fit all the observational constraints. An essential prediction of this model is the existence of a cutoff energy in the range of 5 to 10 GeV.

## 9. Conclusions

Our monitoring of the optical variations revealed the strongest outburst of PKS 0420-014 in 20 years to occur in March, 1992. This epoch coincides with the detection of strong emission of high-energy gamma rays. Lower gamma–ray fluxes and upper limits have been obtained at epochs when the optical fluxes were at a lower level. This correlation indicates that there may be a direct link between gamma–ray outbursts and flares of optically thin synchrotron radiation. The sampling does not enable us to measure any lag, but unless the correlation is a chance coincidence, the delay between the bursts is likely to be less than about a month.

We used the monitoring data to compute spectral indices over wide ranges in frequency from quasi-simultaneous observations. The overall spectrum of the low-energy branch is characteristic of an inhomogeneous jet, with a turnover at about 500 GHz. At lower frequencies the amplitude of historic variations remain independent of frequency down to 1 GHz with little correlation between different frequencies. Throughout the infrared and optical regime the amplitudes seem to increase with frequency, suggesting stronger variations close to the cutoff frequency. The cutoff frequency may vary if the effective Doppler boosting changes with time.

Although poorly sampled, the light curve of the optical emission suggests that variable Doppler boosting may play an important role. Motion on helical trajectories is expected in sources with highly relativistic, magnetic jets. This will lead to a 'lighthouse-effect'. A simple model is capable to qualitatively explain the symmetry and similarity of subsequent outbursts in 1990-1992. This model requires a continuous injection of electrons within the knot and an upper cut-off of the Lorentz factors of the electron population of about 3000.

In such a case the spectral constraints rule out the Synchrotron Self Compton mechanism as a generating mechanism for the high-energy gamma emission. We assume that the gamma–ray flares are due to inverse Compton scattering of ambient photons on the relativistic electrons which are continuously injected within the knot. If the simultaneous flare is actually due to scattering electrons which are already at large distances from the nucleus, hot dust is likely to be the main source of the soft photon field.

*Acknowledgements.* We thank G. Kanbach, T. Krichbaum, M. Tornikoski, E. Valtaoja, and A. Wehrle for discussions and J. Heidt for pointing out an error in an earlier version of the paper. The help of A. Witzel with the VLBI data was invaluable. We also thank H.D. Radecke for an early version of his paper. Literature searches were done in part using the bibliographic data banks of the NED and SIMBAD. This work was supported by the DFG (Sonderforschungsbereich 328). KJS acknowledges support from the EC through grant ERB 4050PL921463.

**Note added in proof:** After this paper was accepted Stevens et al. (1994), to be published in ApJ 437, 91 published detailed mm light curves of 0420 – 014. The 37 GHz data show three bumps, separated by about 13 months, which may correspond to the three optical peaks, if a delay by 9 months is assumed.

## References

Aller, H.G. et al.: 1985, ApJSupp 59, 513
Appl, S. and Camenzind, M.: 1993a, A&A 270, 71 (AC93a)
Appl, S. and Camenzind, M.: 1993b, A&A 274, 699 (AC93b)
Babadzhanyants, M. and Belokon, E.T.: 1986, Astrophysics 23, 639
Balonek, T.J. and Dent, W.A.: 1980, ApJ 240, L3
Bloom, S.D. and Marscher, A.: 1993, in *Compton Gamma–Ray Observatory*, eds. M. Friedlander, N. Gehrels, D.J. Macomb, AIP (N.Y.) Vol. 280, p. 578
Borgeest, U. and Schramm, K.J.: 1994, A&A, 284, 764
Brindle et al.: 1986, MNRAS 221, 739
Brinkmann, W., Siebert, J., and Boller, T.: 1994, A&A 281, 355
Brown, L.M.J. et al.: 1989, ApJ 340, 129
Camenzind, M.: 1993, in *Jets in Extragalactic Radio Sources*, eds. H.–J. Röser & K. Meisenheimer, Lecture Notes in Phys. **421**, 109
Camenzind, M.: 1994, in IAU Symp. **159** *Multi-Wavelength Continuum Emission of AGN*, eds. T.J.–L. Courvosier & A. Blécha, Kluwer, p. 257
Camenzind, M. and Krockenberger, M.: 1992, A&A 255, 59
Chini, R. et al.: 1989, A&A 221, L3
Dent, W.A. et al.: 1979, ApJ 227, L9
Dermer, C.D. and Schlickeiser, R.: 1993, ApJ 416, 458
Dermer, C.D., Schlickeiser, R., and Mastichiadis, A.: 1992, A&A 256, L27
Fichtel, C. et al.: 1994, ApJSupp, 94,551
Gear, W.K. et al.: 1984, ApJ 280, 102
Gear, W.K. et al.: 1985, ApJ 291, 511
Gear, W.K. et al.: 1986, ApJ 304, 295
Ghisellini, G. and Maraschi, L.: 1989, ApJ 340, 181
Ghosh, T. and Gopal-Krishna: 1990, A&A 230, 297
Impey, C. and Neugebauer, G.: 1988, AJ 95, 307
Impey, C. and Tapia, S.: 1990, ApJ 354, 124
Kormendy, J.: 1994, in *Nuclei of Normal Galaxies: Lessons from the Galactic Centre*, ed. A. Harris and R. Genzel, Reidel, in press
Krichbaum, Th. et al.: 1990, A&A 237, 3
Kühr, H. et al.: 1981, A&A Supp. 45, 367
Maraschi, L., Ghisellini, G., and Celotti, A.: 1992, ApJ 397, L5
Marscher, A. and Bloom, S.D.: 1993, in *Compton Gamma–Ray Observatory*, eds. M. Friedlander, N. Gehrels, D.J. Macomb, AIP (N.Y.) Vol. 280
Marscher, A. and Gear, W.K.: 1985, ApJ 298, 114
Michelson, P. et al.: 1994, in *Proc. 2nd Compton Symp.*, eds. C.E. Fichtel, N. Gehrels, J.P. Norris, AIP (N.Y.) Vol. 304, p. 602
Neugebauer, G. et al.: 1984, ApJ 278, L84
Neugebauer, G. et al.: 1986, ApJ 308, 815
Quirrenbach, A. et al.: 1991, ApJ 372, L71
Radecke, H.-D., Bertsch, D.L., Dingus, B.L. et al.: 1995, ApJ 438, 659
Reich, W. et al.: 1993, A&A 273, 65
Schalinski, C.J., 1985, Diploma Thesis, University of Bonn.
Schramm, K.J., et al.: 1993, A&A 278, 391
Sikora, M., Begelman, M.C., Rees, M.J.: 1994, ApJ 421, 153
Smith, A. et al.: 1990, AJ 105, 437
Steppe, H. et al.: 1993 A&A Supp. 102, 611
Teräsranta, H. et al.: A&A Supp. 94, 121
Tornikoski, M. et al.: 1993, AJ 105, 1680
Wagner, S.J.: 1991 in *"Variability of Active Galaxies"*, W.J. Duschl, S.J. Wagner, and M. Camenzind (Eds.), Springer, p. 163
Wagner, S.J. and Witzel, A.: 1992, in *"Extragalactic Radio Sources – From Beams to Jets"*, J. Roland, H. Sol, and G. Pelletier (Eds.), Cambridge University Press, p. 59

Wagner, S.J. et al.: 1993, A&A 271 344
Wehrle, A.E., Cohen, M.H., Unwin, S., Aller, H.D., Aller, M.F., Nicolson, G., 1992, ApJ 391, 589
Wills, B.J. et al.: 1992, ApJ 398, 454
Worrall, D.M. and Wilkes, B.J.: 1990, ApJ 360, 396

This article was processed by the author using Springer-Verlag LaTeX A&A style file version 3.